RSC Advances

ROYAL SOCIETY OF CHEMISTRY

www.rsc.org/advances

Theoretical investigation of dihydroacridine- and diphenylsulphone-derivatives as thermally activated delayed fluorescence emitters for organic light-emitting diodes

Xiaguang Zhang, Wei Shen, Dongmei Zhang, Yongzhen Zheng, Rongxing He, Ming Li*

School of Chemistry and Chemical Engineering, Southwest University, Chongqing 400715, P. R. China

---

* Corresponding author:

E-mail: liming@swu.edu.cn; Phone: +86-023-68253023

Abstract: A series of donor-acceptor-donor type compounds containing 9,9-dimethyl-9,10-dihydroacridine and diphenylsulphone as thermally activated delayed fluorescence emitters are designed and investigated, their broad application prospect in organic light emitting diodes are predicted by density functional theory (DFT). The results show that the orbital interaction of the adjacent atom between acceptor and donor is an important factor to influence the singlet-triplet energy difference. The effective intermolecular singlet-singlet, singlet-triplet and triplet-triplet energy transfer from host to emitters which donor and acceptor linked by C-N bond would be formed. The para- and meta- linked compounds exhibit blue emission and ortho- linked compound show green emission in these emitters.

Keywords: density functional theory, thermally activated delayed fluorescence emitter, singlet-triplet energy differences, donor-acceptor-donor structure

1. Introduction

In organic light-emitting diodes (OLEDs), the holes and electrons recombination produce singlet and triplet excitons, and the ratio of spin statistics is 1:3,[1, 2] so only 25% internal quantum efficiency would be harvested in fluorescent OLEDs.[3] Recently, thermally activated delay fluorescence (TADF) mechanism has been applied to OLEDs.[4, 5] In TADF-OLEDs, the organic emitters which have a small singlet and triplet difference (ΔE_{ST}) can provide a reverse intersystem crossing (RISC) and effectively harvest both singlet and triplet excitons into light, reaching 100% maximum internal quantum efficiency.[6-8] Comparing with phosphorescent OLEDs, the TADF-OLEDs has a strong advantage on reducing the high costs of valuable transition metal, balancing the charge carrier transport and solving unstability of blue transition metal phosphors.[9] Currently, TADF-OLEDs material's study has attracted much attention. However, developing the TADF emitter is a challenging task. On one hand, the compound requires a sufficiently small ΔE_{ST} to ensure triplet excitons that can transfer from triplet state to singlet state. On another hand, it need the appropriate energy level matching of singlet and triplet energy between host and TADF emitter. Deeply understanding the structure-property relationships in TADF emitters is essential to solve above problem.

As the TADF emitter in OLEDs, the type of donor-acceptor (D-A) type or donor-acceptor-donor (D-A-D) is a trends in current research.[10, 11] Generally, it has a small spatial overlap between HOMO and LUMO for donor and acceptor structure, which can contribute to inducing intramolecular charge transfer, leading a small exchange integral between donor and acceptor, causing a small singlet–triplet splitting, namely small ΔE_{ST}. Based on this concept, Adachi's group has chosen various donors and acceptors to design TADF emitters applied in OLED, consequently, high external electroluminescence quantum efficiency (EQE) are achieved.[12-14] Among the synthesized TADF materials, diphenylsulphone and acridine derivatives are always used for donor and acceptor, and they showed an excellent molecule performances. For example, bis[4-(3,6-dimethoxycarbazole)phenyl]sulfone has a small ΔE_{ST} (0.21 eV). As an emitter, the OLED device shows an excellent maximum EQE of 14.5% and reduces efficiency roll-off.[15] The highly efficient TADF performance of Spiro-acridine has been demonstrated, and it exhibits a high internal photoluminescence efficiency value (67.3%).[16] The device with 9,10-dihydroacridine and diphenylsulphone derivative as emitter can exhibit a high EQE (19.5%), the value is so high that they can be comparable with the best phosphorescent OLEDs in performance.[12] Additionally, Adachi's group demonstrated that the small ΔE_{ST} and large fluorescence rate (k_{F}) can be achieved by increasing the distance between donor and acceptor in intramolecular-charge-transfer molecules.[17] At the same time, many studies show that the increasing steric hindrance between donor and acceptor can also lead to spatially separation of the frontier orbitals, and the higher photoluminescence quantum yields appeared in the D-A-D-type molecules, rather than the D-A-type molecules.[18, 19]

Herein, we have performed density functional theory (DFT) to investigate a series of TADF-emitters based on D-A-D electronic structure, comprising diphenylsulphone electron acceptor core units substituted with electron donor units of 9,9-dimethyl-9,10-dihydroacridine (**Figure 1**). In addition, to verify the molecule properties of TADF emitters calculated above, *m*-bis(*N*-carbazolyl)benzene (mCP), 4,4'-bis(carbazole-9-yl)biphenyl (CBP) and bis(2-(diphenylphosphino)phenyl)ether oxide (DPEPO) are selected as reference host materials. In this work, we theoretically predict the application prospect of the studied compounds in TADF-OLEDs based on the ΔE_{ST} and intermolecular energy transfer between host and emitter. Our goal is to investigate the TADF mechanism of energy transfer in the host-guest system, analyze the influence of the different linkage style of carbon-nitrogen (para-, meta- and ortho-) and carbon-carbon (para-, meta- and ortho-) between donor and acceptor on molecular performance.

2. Computation Details

In this work, in order to select a reliable method to study the ground and excited states of investigated system, different Density functional theory (DFT) methods were employed with 6-31G(d) and 6-311+G(d) basis set (the results are list in Electronic Supplementary Information). Frequency calculations showed that the optimized structures are minimum energy on the potential energy surfaces. In this paper, the MAXimum deviation (MAX), the Mean Absolute Deviation (MAD), the Root Mean-Squared Deviation (RMSD), and the relative error (*E*r) have been used as a guaid for comparison between experimental and calculated values.[20] The parameters defined as

$$\mathrm{MAX} = \max\left\{ \left| x_i \right| \right\} \tag{1}$$

$$\mathrm{MAD} = \frac{1}{n}\sum_i^n \left| x_i \right| \tag{2}$$

$$\mathrm{RMSD} = \sqrt{\frac{1}{n}\sum_i^n \left| x_i \right|^2} \tag{3}$$

$$E_r = \frac{x_i}{\Omega_i^{\exp erimental}} = \frac{\Omega_i^{calculated} - \Omega_i^{\exp erimental}}{\Omega_i^{\exp erimental}} \tag{4}$$

where Ω is the corresponding energies.

The impact on geometries of ground (S_0) and triplet (T_1) states with different functionals and basis set (see **Table S1)** were discussed. The geometry of T_1 state is optimized via spin-unrestricted DFT level, and the triplet energy (E_T) also corrected for zero-point energies. With 6-31G(d) basis set, the HOMO and E_T produced the smallest MAX, MAD and RMSD (0.01, 0.00 and 0.007, respectively) with B3P86 functional. With 6-31+G(d) basis set, the HOMO produced the smallest *E*r with M06 method. Accordingly, the calculated results with B3P86/6-31G(d) level[21] are excellent consistent with the experiment data (**Table S2**). Generally, it is difficult to describe the virtual orbitals theoretically than occupied orbital. If the main transition of the first excitation state originates from HOMO to LUMO, the LUMO energy can be obtained from HOMO energy plus the first vertical excitation energy. Vertical absorption and emission energies can obtain through time-dependent density functional theory (TD-DFT) calculation based on optimized S_0 and the first singlet excited (S_1) state geometries, respectively. Combined the HF exchange percentage (HF%)[22] and the impact of the solvent effect, many functionals which possess different HF% in toluene (by using the polarized continuum model (PCM)[23]) and gas phase were performed, respeectively (see **Table S1** and **S3)**. One can find that the results with TD-B3LYP/6-31G(d)//B3P86/6-31G(d)[24] in toluene can obtain a more accurate excitation energies and LUMO when compare with the experiment data (the MAD and RMSD is 0.047 and 0.047, respectively). From **Table S4**, calculated by TD-B3LYP/6-31G(d) in toluene can obtain a more accurate emission wavelength (Er = 2.14 %). All the calculations are performed by Gaussian09 program.[25]

3. Results and discussion

3.1. Geometry structures of the optimized ground and singlet excited states

The structure parameter of compound is a key factor that contributes to understand the radiative transition of molecule, the selected bond lengths and dihedral angle of compounds in ground (S_0) and singlet excited (S_1) state are collected in **Table 1**,

Table S5 and **Figure S1**. For C-N linkage series, the dihedral angle between donor (9,9-dimethyl-9,10- dihydroacridine) and phenyl plane of acceptor (diphenylsulphone) are over 75°, which shows that the steric effect in the ground states are far away from 0°. A large dihedral angle could limit the coupling between the donor and acceptor in S_0 state. The natural bond orbital analysis shows that the nitrogen atoms adopt sp^2 hybridized orbital, while the bond between nitrogen atom (donor) and carbon (acceptor) is a weak p-π conjugation, leading the bond length of nitrogen-carbon between the nitrogen-carbon single bond length (1.54 Å) and nitrogen-carbon conjugation bond length (1.37 Å), which indicates a small bond energy. According to the high binding energy between donor and acceptor, a linkage bond, which length is between the carbon-carbon single bond length (1.54 Å) and carbon-carbon double bond length (1.34 Å), in C-C linkage series is found comparing with the C-N linkage series. In addition, the linkage position (ortho-, meta-, para-) has a great influence on the structure parameter of C-C linkage series (dihedral angle para- ≈ meta- > ortho-). In excited state, the steric effect also limits the flattening distortion of compounds C-N linkage series, while the C-C linkage series has an obvious planarization tendency. Higher Franck-Condon factor will be formed accompanied with the structural deformation of the excited and ground state, which leads to highly effective nonradiative relaxation channel.[26, 27] Results showed that radiative transition properties of C-N linkage series is more effective than that of the C-C ones.

In ground state, the large torsion angle between donor and acceptor plays an important role in separating the highest occupied molecular orbital (HOMO) and the lowest unoccupied molecular orbital (LUMO). The HOMO and LUMO of compounds are depicted in **Figure 2**. Due to the large dihedral angle between the donor and acceptor, the molecules of C-N linkage series show a small spatial overlap between HOMO and LUMO orbitals. While the HOMO orbital of C-C linkage series tend to delocalized over the conjugated area, thus, the HOMO and LUMO orbitals exhibit a large orbital overlap. In addition, the density of states and projected density of states are calculated to test the orbital overlap degree, related results are showed in **Figure S2**. For C-N linkage series, the densities of HOMO are localized on the donor, and occupy values for the electronic transitions module exceed 95% (para-, meta- and ortho- are 97.3%, 97.0% and 96.3%, respectively), while the densities of LUMO are localized on acceptor, and occupy values of para-, meta- and ortho- are 96.8%, 97.8%, 97.2%, respectively. Relatively, for the C-C linkage series, the donor occupy values of HOMO for para-, meta- and ortho- are 89.9%, 92.1% and 95.9%, respectively, and the corresponding densities on LUMO localized on acceptor occupy values are 75.3%, 92.0%, 94.2%, respectively. The results show that the dihedral angle increases with the overlap degree declines of the HOMO and LUMO for C-C linkage series (overlap degree para- > meta- > ortho-).

Based on above analysis, C-N linkage series have larger torsion angles between donor and acceptor than C-C linkage series, and show a smaller spatial overlap between HOMO and LUMO orbitals.

3.2. Singlet and triplet excitation energy

In order to examine the electronic transition nature of compounds, TD-DFT calculations are implemented. The results are collected in **Table S6**, as shown, the HOMO → LUMO character has predominated in the transition of $S_0 \rightarrow S_1$. In general, the nature transition orbital is equal to the HOMO and LUMO when the probability is over 90%, and the natural transition orbitals for the $S_0 \rightarrow S_1$ and $S_0 \rightarrow T_1$ are displayed in **Figure S3**. For C-N linkage series, the hole is located on the donor, and the particle is located on the acceptor. While, for C-C linkage series, the hole and particle of compounds have relatively large orbital overlap, the results are similar to the HOMO/LUMO analysis. The transition state of $S_0 \rightarrow S_1$ in C-N linkage series is an obvious intramolecular charge transfer state, so the compounds 1-3 have small transition energy of $S_0 \rightarrow S_1$. In general, it is necessary for the efficient thermally activated delayed fluorescence (TADF) emitter that there is a small energy difference between the first excited singlet and triplet states (that is ΔE_{ST}). The ΔE_{ST} values of compounds are collected in **Table 2**. The values of ΔE_{ST} in C-N linkage series are much less than that of C-C linkage series, the small orbital overlap between hole and particle in C-N linkage series leads to the low orbital overlap integral between ϕ and ϕ^*, that is a weak exchange integral $J(\phi, \phi^*)$. As shown in **Equation 5**,[28-30] the degree of spatial overlap will strongly alter the value of ΔE_{ST}. The up-conversion process of $T_1 \rightarrow S_1$ in C-N linkage series is thermodynamically favorable, because the small ΔE_{ST} enables a faster reverse intersystem crossing (RISC) rate of $T_1 \rightarrow S_1$ than that of non-radiation decay of $T_1 \rightarrow S_0$. According to the energy gap law, the rate of internal conversion exceeds the intersystem crossing rate or the RISC rate, so the process of RISC occurs between S_1 and T_1 states. As the ΔE_{ST} of C-C linkage series is large, the up-conversion from T_1 to S_1 is difficult. In addition, the compounds also possess high ΔE_{ST} in the higher-order excited states, which means that the compounds of C-C linkage series no TADF would occur.

$$\left.\begin{aligned}
&\Delta E_{ST} = E(\mathrm{S}) - E(\mathrm{T}) = 2J(\phi,\phi^*) \\
&J(\phi,\phi^*) = \left\langle \phi(1)\phi^*(2) \left| \frac{e^2}{r_{1,2}} \right| \phi(2)\phi^*(1) \right\rangle \\
&J(\phi,\phi^*) \approx \frac{e^2}{r_{1,2}} \left\langle \phi(1)\phi^*(2) | \phi(2)\phi^*(1) \right\rangle \approx \left\langle \phi | \phi^* \right\rangle
\end{aligned}\right\} \tag{5}$$

As is known to all, the small ΔE_{ST} which resulted from the large dihedral angle between donor and acceptor of compounds may lead to the occurance of the efficient TADF emission. Why compound 6 which possesses a large dihedral angle (~60°) between donor and acceptor has a large ΔE_{ST}? It can be explained that the stronger electron donating ability of the molecules with the C-N linkage (the natural population analyses charge of donor of 1-3 and 6 are 0.39, 0.38, 0.37 and 0, respectively). In addition, we also scanned the torsion angle between donor and acceptor of compounds 1-3 and 6 to explore its influence on the value of ΔE_{ST}.[31] The results are collected in **Table S7.** In compounds 1-3, when the dihedral angles approximate to 0°, the HOMO is localized on the full molecular structure, and the LUMO is mainly localized on the π*-orbitals of the acceptor. And the excited singlet states largely come from HOMO → LUMO. The dihedral angle has a great influence on energy of $S_0 \rightarrow S_1$, and the large spatial overlap lead to a large ΔE_{ST}. At the same time, the small dihedral angle leads to a strong p-π conjugation of nitrogen-carbon between donor and acceptor, which help to increase the intramolecular interaction.

Consequently, the compounds of 1-3 have no TADF emission occurs when the dihedral angles approximate to 0°. For compound 6, when the dihedral angle is 0°, the HOMO is localized on the full molecular structure, and the LUMO is mainly localized on the acceptor. The ΔE_{ST} is 0.46 eV, the value are similarly to the ΔE_{ST} of compound 6 when the dihedral angle is 60°. When the dihedral angle is 90°, the large spatial overlap between HOMO and LUMO is also realized, leading to a large ΔE_{ST}, thus, no TADF emission occurs. The carbon-carbon bond has a large $\pi\pi$ conjugation no matter how large dihedral angle between donor and acceptor in compound 6. Namely, the obvious spatial overlap lead to large ΔE_{ST}.

In summary, C-C linkage series compounds have large ΔE_{ST}, which lead C-C linkage series compounds to be unsuitable as a TADF emitter. In addition, the orbital interaction of the adjacent atom between acceptor and donor is an essential factor which has an impact on the value of ΔE_{ST}.

3.3. Energy and charge transfer between emitter and host

In order to avoid concentration quenching and ensure highly efficient electroluminescence, the TADF emitters are usually dispersed in a suitable host material which has higher triplet energy (E_{T}) than that of emitter to avoid reversing energy transfer from host to emitter.[32] In this work, mCP, CBP and DPEPO are selected as host materials. In view of the C-C linkage series are unsuitable as TADF emitter, so we only discuss the compounds of C-N linkage series. **Table 2** shows that the E_{T} of host molecule CBP (2.73 eV) is smaller than emitter compounds 1 (2.92 eV) and 2 (2.98 eV), so compounds 1 and 2 dispersed in CBP are unsuitable. Meanwhile the results also verify the experiment conclusion that the PLQY of compound 1 can increase when change host from CBP to mCP to DPEPO.[12] In general, singlet and triplet excitons generate from electron-hole recombination in host. Singlet excitons from host transfer into the singlet state of the emitter by Förster energy transfer process.[33] Triplet excitons from host transferred into the singlet state or triplet state of the emitter by Dexter energy transfer process.[34] The transition of $T_1 \rightarrow S_0$ in host molecules CBP, mCP and DPEPO is spin forbidden, and the calculated transition dipole moment (**Table S8**) of host show that the transition $S_1 \rightarrow S_0$ of DPEPO is slightly allowed, which verify the experiment conclusion again. The transition energy of S_1 and T_1 in host and emitter (**Table 2**) show that it is thermodynamics favorable and engender prompt fluorescence emission that $S_1 \rightarrow S_1$ intermolecular Förster energy transfer from DPEPO to emitters 1, 2 and 3. As can be seen from the transition energy, the singlet excitation energy $E(S_1)$ and triplet excitation energy $E(T_1)$ of emitters 1, 2 and 3 are smaller than $E(T_1)$ of host molecule DEPEO, which demonstrate the $T_1 \rightarrow S_1$ Förster energy transfer and $T_1 \rightarrow T_1$ Dexter energy transfer from DEPEO to emitters also belong to the thermodynamics favorable. Moreover, the emitter 1 and 3 dispersed in host molecule CBP and mCP, respectively. It can engender $S_1 \rightarrow S_1$ intermolecular Förster energy transfer and $T_1 \rightarrow T_1$ Dexter energy transfer, viewed from the thermodynamics point. Besides, the good overlap of host emission and emitter absorption could effectively demonstrate the Förster energy transfer which is a long-range energy transfer. **Figure 3** shows that the absorption wavelength of emitters (1, 2 and 3 are 420.17 nm, 414.18 nm and 431.50 nm, respectively) and the emission wavelength of DPEPO (403.72 nm) show the good spectrum overlap between host emission and emitter absorption.

In addition, balanced charge transport and fast charge transport rates are important performance for TADF emitter. Form Marcus-Hush equation show that low reorganization energy (λ) and high transfer integral (V) could lead to high charge mobility rate [35], and λ is a main influential factors. **Table S9** shows that the monotonous increase of λ_h in C-N linkage series compounds 1 (para-) < 2 (meta-) < 3 (ortho-) that hole transfer rate is 3 (ortho-) < 2 (meta-) < 1 (para-), the increase monotonously of λ_e and Ve in C-N linkage series compounds 1 (para-) < 2 (meta-) < 3 (ortho-) and 3 (ortho-) < 2 (meta-) < 1 (para-) that electron transfer rate is 3 (ortho-) < 2 (meta-) < 1 (para-). The results show that compound 1 (para-) has the fastest charge transfer rate in C-N linkage series compounds. The values of λ_h/λ_e increase as the following: 3 (ortho-) < 2 (meta-) < 1 (para-), demonstrating that the 1 (para-) exhibit a good balanced charge (hole and electron) transport capacity.

From above discussion, DPEPO as a host molecule suited all emitter, the CBP also conforms to the requirement of emitter 3. In addition, the effective energy transfer would be formed between host and emitter. And the C-N linkage series have a good balance with the charge transport performance and fast charge transport rate, in addition, 1 (para-) exhibits the best charge transport performance.

3.4. Potential device performances used in OLED

A low energy barrier for charge injection from the neighboring layers is the basic requirement for design of OLED, so the characters of higher HOMO and lower

LUMO energy levels than that of the host are desired for the emitter to ensure efficient direct change trapping on emitting layer. Comparing with host molecule DPEPO, the energies of frontier molecular orbitals (**Table 2**) of C-N linkage series are meet direct charge trapping demand.[36] The energy of the HOMO level increases monotonously in the compounds 3 (ortho-) < 2 (meta-) < 1 (para-). Hence, hole transfer from host DPEPO to emitter 3 would be more facile than other emitters. For electron injection, the changes of energy of LUMO level are not obvious, and the increase monotonously in compounds 1 (para-) < 2 (meta-) < 3 (ortho-), and 2 (-2.89 eV) and 3 (-2.86 eV) have similar LUMO energy levels. The results show that all compounds have the similar electron-injection barrier. Further ionization potentials (IP) and electron affinities (EA) are consistent with above result **(Table S9)**. Thus, 3 (ortho-) have an appropriate charge injection performance.

The design of different emitters (1, 2 and 3) also shows a good potential performance due to the small ΔE_{ST} relative to a device performance. **Table 3** shows that the maximum emission wavelength of compounds 1, 2 and 3 are found to be 471.08 nm, 475.19 nm and 617.28 nm, respectively. The 1 and 2 exhibit a blue emission, and 3 exhibit a green emission.

From the combination property of charge injection barrier and device turn-on voltage, all compounds show good performances when choose them as a blue or green TADF-OLED emitter. And among the C-N linkage series in our work, compound 1 appears to be the most promising blue emission molecule, and 3 is a good green emission molecule.

4. Conclusion

In this work, a comprehensive theoretical investigation has been performed to study on the D-A-D electronic structure of C-N linkage series and C-C linkage series. According to the geometry structure between ground state and singlet excited state, the value of ΔE_{ST} and orbital overlap of donor and acceptor in $S_0 \rightarrow S_1$ transition of two series compounds can be found that the C-C linkage series compounds couldn't suit to be TADF emitter. The results of scan torsion angle between donor and acceptor show that the influential factor of the value of ΔE_{ST} is the orbital interaction of the adjacent atom between acceptor and donor. From the triplet energy and the transition energy of emitters and host analysis, we can see that the DPEPO is the best suitable host molecule for all series emitter of C-N linkage compounds, and effective energy transfer of $S_1 \rightarrow S_1$, $T_1 \rightarrow S_1$ and $T_1 \rightarrow T_1$ from DEPEO to emitters would be formed. Moreover, from the HOMO/LUMO energy could infer that the direct charge trapping would be formed on emitter layer. Furthermore, good performance and high RISC of C-N linkage series compounds can be expected due to the low ΔE_{ST}. C-N linkage series compounds, 1 (para-) and 2 (meta-) exhibits blue emission, and 3 (ortho-) exhibits green emission. We believe that our study could provide instructive information for experimental and theoretical investigation in TADF-OLED.

References

1. C. W. Tang and S. VanSlyke, *Applied physics letters*, 1987, 51, 913-915.
2. M. Pope, H. Kallmann and P. Magnante, *The Journal of Chemical Physics*, 1963, 38, 2042-2043.
3. M. Baldo, D. O'brien, Y. You, A. Shoustikov, S. Sibley, M. Thompson and S. Forrest, *Nature*, 1998, 395, 151-154.
4. K. Goushi, K. Yoshida, K. Sato and C. Adachi, *Nature Photonics*, 2012, 6, 253-258.

5. A. Endo, M. Ogasawara, A. Takahashi, D. Yokoyama, Y. Kato and C. Adachi, *Advanced Materials*, 2009, 21, 4802-4806.
6. Q. Zhang, J. Li, K. Shizu, S. Huang, S. Hirata, H. Miyazaki and C. Adachi, *Journal of the American Chemical Society*, 2012, 134, 14706-14709.
7. H. Uoyama, K. Goushi, K. Shizu, H. Nomura and C. Adachi, *Nature*, 2012, 492, 234-238.
8. Y. Tao, K. Yuan, T. Chen, P. Xu, H. Li, R. Chen, C. Zheng, L. Zhang and W. Huang, *Advanced Materials*, 2014, 26, 7931-7958.
9. S. Y. Lee, T. Yasuda, Y. S. Yang, Q. Zhang and C. Adachi, *Angewandte Chemie*, 2014, 126, 6520-6524.
10. R. Ishimatsu, S. Matsunami, T. Kasahara, J. Mizuno, T. Edura, C. Adachi, K. Nakano and T. Imato, *Angewandte Chemie International Edition*, 2014, 53, 6993-6996.
11. F. B. Dias, K. N. Bourdakos, V. Jankus, K. C. Moss, K. T. Kamtekar, V. Bhalla, J. Santos, M. R. Bryce and A. P. Monkman, *Advanced Materials*, 2013, 25, 3707-3714.
12. Q. Zhang, B. Li, S. Huang, H. Nomura, H. Tanaka and C. Adachi, *Nature Photonics*, 2014, 8, 326-332.
13. M. Uejima, T. Sato, M. Detani, A. Wakamiya, F. Suzuki, H. Suzuki, T. Fukushima, K. Tanaka, Y. Murata and C. Adachi, *Chemical Physics Letters*, 2014, 602, 80-83.
14. T. Komino, H. Tanaka and C. Adachi, *Chemistry of Materials*, 2014, 26, 3665-3671.
15. S. Wu, M. Aonuma, Q. Zhang, S. Huang, T. Nakagawa, K. Kuwabara and C. Adachi, *J. Mater. Chem. C*, 2013, 2, 421-424.
16. G. Méhes, H. Nomura, Q. Zhang, T. Nakagawa and C. Adachi, *Angewandte Chemie International Edition*, 2012, 51, 11311-11315.
17. Q. Zhang, H. Kuwabara, W. J. Potscavage, S. Huang, Y. Hatae, T. Shibata and C. Adachi, *Journal of the American Chemical Society*, 2014, 136, 18070-18081.
18. J. Lee, K. Shizu, H. Tanaka, H. Nomura, T. Yasuda and C. Adachi, *Journal of Materials Chemistry C*, 2013, 1, 4599-4604.
19. W. Li, Y. Pan, R. Xiao, Q. Peng, S. Zhang, D. Ma, F. Li, F. Shen, Y. Wang and B. Yang, *Advanced Functional Materials*, 2014, 24, 1609-1614.
20. M. Moral, L. Muccioli, W.-J. Son, Y. Olivier and J. C. Sancho-García, *Journal of Chemical Theory and Computation*, 2014, 11, 168-177.
21. J. Perdew, *Phys. Rev. B*, 1986, 34, 7406-7406.
22. S. Huang, Q. Zhang, Y. Shiota, T. Nakagawa, K. Kuwabara, K. Yoshizawa and C. Adachi, *Journal of Chemical Theory and Computation*, 2013, 9, 3872-3877.
23. G. Scalmani and M. J. Frisch, *The Journal of chemical physics*, 2010, 132, 114110.
24. A. D. Becke, *The Journal of Chemical Physics*, 1993, 98, 5648-5652.
25. G. W. T. M. J. Frisch, H. B. Schlegel, G. E. Scuseria, M. A. Robb, J. R. Cheeseman, G. Scalmani, V. Barone, B. Mennucci, G. A. Petersson, H. Nakatsuji, M. Caricato, X. Li, H. P. Hratchian, A. F. Izmaylov, J. Bloino, G. Zheng, J. L. Sonnenberg, M. Hada, M. Ehara, K. Toyota, R. Fukuda, J. Hasegawa, M. Ishida, T. Nakajima, Y. Honda, O. Kitao, H. Nakai, T. Vreven, J. A. Montgomery, Jr., J. E. Peralta, F. Ogliaro, M. Bearpark, J. J. Heyd, E. Brothers, K. N. Kudin, V. N. Staroverov, R. Kobayashi, J. Normand, K. Raghavachari, A. Rendell, J. C. Burant, S. S. Iyengar, J. Tomasi, M. Cossi, N. Rega, J. M. Millam, M. Klene, J. E. Knox, J. B. Cross, V. Bakken, C. Adamo, J. Jaramillo, R. Gomperts, R. E. Stratmann, O. Yazyev, A. J. Austin, R. Cammi, C. Pomelli, J. W. Ochterski, R. L. Martin, K. Morokuma, V. G. Zakrzewski,

G. A. Voth, P. Salvador, J. J. Dannenberg, S. Dapprich, A. D. Daniels, O. Farkas, J. B. Foresman, J. V. Ortiz, J. Cioslowski, and D. J. Fox, *Inc.: Pittsburgh, PA*, 2009.

26. N. Turro and M. M. Photochemistry, *Menlo Park, CA*, 1978, 317-319.
27. C. L. Linfoot, M. J. Leitl, P. Richardson, A. F. Rausch, O. Chepelin, F. J. White, H. Yersin and N. Robertson, *Inorganic chemistry*, 2014, 53, 10854-10861.
28. N. J. Turro, *Modern molecular photochemistry*, University Science Books, 1991.
29. T. Ziegler, A. Rauk and E. J. Baerends, *Theoretica chimica acta*, 1977, 43, 261-271.
30. Y. Pan, W. Li, S. Zhang, L. Yao, C. Gu, H. Xu, B. Yang and Y. Ma, *Advanced Optical Materials*, 2014, 2, 510-515.
31. M. J. Leitl, V. A. Krylova, P. I. Djurovich, M. E. Thompson and H. Yersin, *Journal of the American Chemical Society*, 2014, 136, 16032-16038.
32. M. A. Baldo, C. Adachi and S. R. Forrest, *Physical Review B*, 2000, 62, 10967.
33. T. Főrster, *Discuss. Faraday Soc.*, 1959, 27, 7-17.
34. D. L. Dexter, *The Journal of Chemical Physics*, 1953, 21, 836-850.
35. R. A. Marcus, *Reviews of Modern Physics*, 1993, 65, 599-610.
36. H. Suzuki and S. Hoshino, *Journal of applied physics*, 1996, 79, 8816-8822.

Table 1. Bonds lengths (Å) and dihedral angles (°) between donor and acceptor in ground state. All calculation is obtained by B3P86/6-31G(d) level.

compound		bond length/Å		dihedral angle/°	
1	S_0	1.4265	1.4265	-76.4372	-77.7945
2	S_0	1.4260	1.4261	77.6548	78.5084
3	S_0	1.4265	1.4265	-77.1852	-77.1719
4	S_0	1.4748	1.4751	-35.1964	35.0320
5	S_0	1.4762	1.4763	-35.5985	34.9405
6	S_0	1.4859	1.4857	-61.3863	-55.1947

Table 2. Frontier molecular orbital energy (eV), triplet energy (eV) and transition energy (eV) of compounds, among them Frontier molecular orbital energy and triplet energy calculation by B3P86 functional and the transition energy calculation by B3LYP functional in 6-31G(d) basis set.

compound	HOMO	LUMO[a]	E_T	$E(S_1)$	$E(T_1)$	ΔE_{ST}
1	-5.92	-2.97/2.92[b]	2.92	2.95	2.94	0.01
2	-5.88	-2.89	2.98	2.99	2.97	0.02
3	-5.73	-2.86	2.69	2.87	2.85	0.02
4	-5.86	-2.59	2.91	3.27	2.78	0.49
5	-5.83	-2.39	2.67	3.44	2.92	0.52
6	-5.77	-2.24	2.84	3.53	3.15	0.38
mcp	-6.08	-2.06	3.19/2.90[b]	4.02	3.21	0.81
dpepo	-6.65	-1.94	3.25/3.30[b]	4.71	3.59	1.12
cbp	-5.98	-2.38	2.73/2.64[b]	3.60	2.99	0.61
donor[c]	-5.74	-1.36	3.29	4.38	3.43	0.95
acceptor[d]	-7.78	-2.65	3.92	5.13	3.64	1.49

[a] LUMO= $E(S_1)$-HOMO; [b] experimental date, ref. 10; [c] donor is 9,9-dimethyl-9,10-dihydroacridine; [d] acceptor is diphenylsulphone

Table 3. Calculated emission wavelength (nm) and emission energy (eV) of compounds 1-3. All calculation is obtained by B3LYP/6-31G(d) level.

compound	Wavelength	E
1	471.08	2.63
2	475.19	2.61
3	617.28	2.11

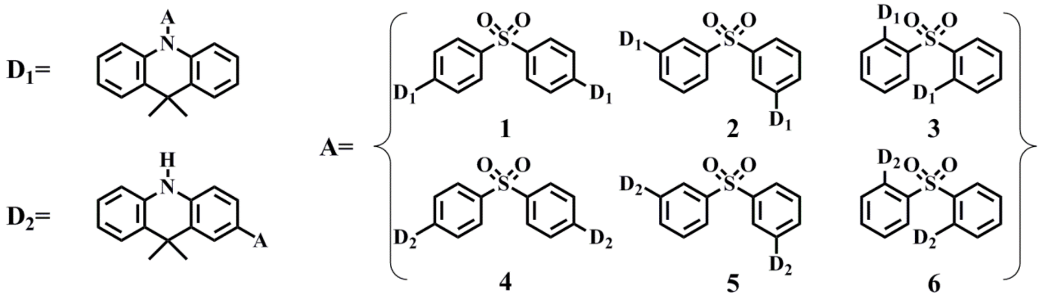

Fig. 1. Molecular structures of compounds 1-6.

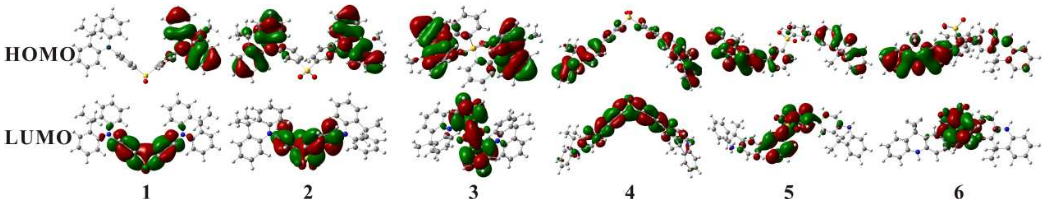

Fig. 2. Frontier molecular orbitals for compounds 1-6 in the ground state.

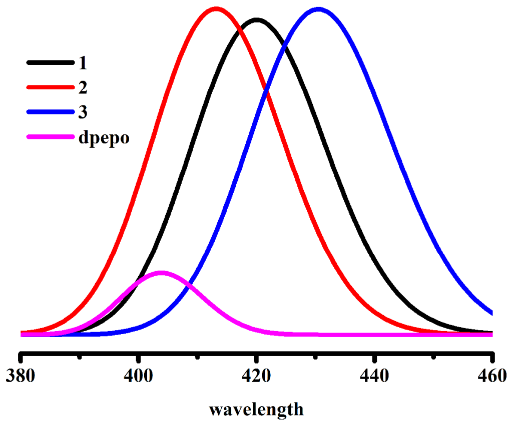

Fig. 3. Emitter's (1, 2 and 3) absorption spectra and host's (dpepo) emission spectra.